Supporting Information

A Photofunctional Platform of Bis-terpyridine Ruthenium Complex-Linked Coordination Polymers with Structural Diversity

Aichun Wu, Yuanlin Tang, Xinling Li, Baohua Zhang, Aiju Zhou, Zhiwei Qiao, Lianpeng Tong**

School of Chemistry and Chemical Engineering, Guangzhou University, No. 230 Wai Huan Xi Road, Higher Education Mega Center, Guangzhou, 510006, P. R. China.

*Email: ltong@gzhu.edu.cn (L. Tong), zqiao@gzhu.edu.cn (Z. Qiao)

Table of Contents

General Methods and Materials.

Complex bis(4′-carboxyl-2,2′:6′,2″-terpyridine) Ru(II) hexafluorophosphate, $[Ru(tpyCOOH)_2](PF_6)_2$, was prepared according to the literature method.[1] Other solvents and chemical materials for syntheses were purchased from commercial sources and used as received without further purification, except n-tertbutyl ammonium hexafluorophosphate which was purified by recrystallization in ethanol for three times. Water used in the syntheses or analysis was purified by Milli-Q technique (18.2 MΩ). The 5% Nafion resin solution was purchased from Sigma Aldrich (product no. 274704).

The pH values of solution were measured by Mettler Toledo pH meter (S210). The C, H, and N element analysis was conducted on the Vario EL Cube elemental analyzer. The powder X-ray diffractometer (PXRD) was measured in the 2θ angular range from 5° to 50° at 273 K using Rigaku MiniFlex600 equipped with a Cu $K\alpha$ microsource. Thermalgravimetric analysis (TGA) was carried out on PerkinElmer TGA4000. The ramp rate of temperature elevation is 10 K per min from room temperature to 500 ℃. Field-emission scanning electron microscopy (FE-SEM) images were taken by JEOL JSM-7001F with an accelerating voltage of 15 kV. Transmission electron microscope (TEM) images were taken by JEOL JEM-2100F. UV-vis spectra were collected by SHIMADZU UV3600 PLUS spectrometer. Gas sorption experiments were carried out using Micromeritics ASAP 2460 system. The steady-state photoluminescent emission or excitation spectra of solid samples were measured using Edinburgh FLS1000 in an ambient condition, with a Xe_2 xenon lamp as a powerful triggering light source. The powder samples were positioned into a homemade quartz slide with a capping layer, upon which the photophysical measurements were conducted. The time-resolved photoluminescent experiments were conducted by using Edinburgh FLS1000 and the samples were excited by a picosecond pulsed LED (EPLED-365) light source (365 nm as excitation wavelength). The inductively coupled plasma atomic mass spectrometry (ICP-MS, NexION 300) was used to measure the element content in bimetallic coordination polymer. The XPS analyses were carried out on a PHI 5000 Versa Probe III spectrometer using monochromatic Al $K\alpha$ X-ray source. Survey scan analyses were carried out by scanning a 200 μm X-ray beam over a 500×500 microns area. The analyzer pass energy and step size were selected as 280.0 eV and 1.0 eV. High resolution analyses were carried out with a similar X-ray beam setting and analysis area, and the analyzer pass energy and step size were selected to be 69.0 eV and 0.125 eV, respectively. The energy for all the spectra had been corrected on the base of carbon 1s peak set to be 284.8 eV. The acquired data were analyzed using PHI MultiPak software.

The electrochemical measurements were performed on a CHI 660e A18921 potentiostat/galvanostat with a built-in electrochemical impedance spectroscopy (EIS) module. A conventional three-electrode cell was used for electrochemical study, including a glassy carbon working electrode (ø = 3 mm, in a PEEK sheath), a platinum wire counter electrode, and a Ag/Ag^+ (in acetonitrile electrolyte) reference electrode.

Prior to application, the glassy carbon working electrode was first polished with 2500 grit silicon carbide sandpaper, and then was polished with 1.0 μm and 0.05 μm Al_2O_3 paste in sequence on a wet polishing cloth. The glassy carbon electrode was ultrasonicated in ethanol and water for 30 s, respectively, in order to remove Al_2O_3 particle residue on the surface. Ferrocene was used as an internal reference. For preparation of the CP-loaded electrode, 2 mg CP solid sample, 480 μL deionized water, 480 μL ethanol and 40 μL Nafion were mixed and sonicated for half hour. A volume of 5 μL dispersion was drop-coated onto the clean glassy carbon electrode. The treated electrode was dried under an infrared lamp for 1 hour, affording the CP-modified working electrode with the loading sample amount of 67.94 μg cm^{-2}.

Syntheses of Coordination Polymers.

Synthesis of Ni(II)/Co(II) bimetallic coordination polymers (**Ni_x-Co_y-Ru**, x/y=1/1, 1/2, 1/4, and 1/6). The bimetallic coordination polymers were prepared by following the procedure in the literature.[1] The $Co(NO_3)_2{\cdot}6H_2O$ and $Ni(ClO_4)_2{\cdot}6H_2O$ salts with different stoichiometric ratios ($n_{Co} + n_{Ni}$= 0.05 mmol) and $[Ru(tpyCOOH)_2](PF_6)_2$ (0.025 mmol, 0.024 g) were dissolved in DMF (5 mL). The solution was transferred into a teflon-lined steel autoclave and heated at 120℃ for 24h. The crystalline solid were collected by filtration, washed with DMF and EtOH sequentially for three times and soaked in CH_2Cl_2 for three days. The CH_2Cl_2 solvent was changed once per day. The solid products denoted as **Co_x-Ni_y-Ru** (x/y=1/1, 1/2, 1/4, and 1/6) were dried under vacuum at 80 ℃ overnight.

Synthesis of the Cu(II) coordination polymer (**Cu-Ru**). A 5 mL glass solvothermal vial was charged with $CuCl_2{\cdot}2H_2O$ (0.0034 g, 0.02 mmol), $[Ru(tpyCOOH)_2](PF_6)_2$ (0.0096 g, 0.01 mmol), 0.8 mL DMF and 1.2 mL EtOH. The mixture formed a homogenous solution at room temperature. The vial was placed and kept in a heating oven at 80 ℃ for 36 hours. After cooling to room temperature, red cuboid crystals suitable for single crystal X-ray diffraction was obtained (2.8 mg), yield = 51.2% according to the mole amount of $[Ru(tpyCOOH)_2](PF_6)_2$. The cuboid crystals were washed with DMF for three times and soaked in EtOH for three days. The EtOH solvent was changed once per day. The solid crystals was collected and dried under vacuum at 60 ℃ overnight. Elemental analysis (%) of $\{2Cu{\cdot}2[Ru(tpyCOO^{-})_2]{\cdot}2DMF{\cdot}Cl{\cdot}3PF_6{\cdot}7.5H_2O\}$, calcd. for $C_{70}H_{69}F_{18}N_{14}O_{17.5}P_3Ru_2Cu_2$: C, 38.46; H, 3.18; N, 8.97; found: C, 38.16; H, 3.02; N, 9.10.

Synthesis of the Eu(III) coordination polymer (**Eu-Ru**). A 5 mL glass solvothermal vial was charged with $Eu(NO_3)_3{\cdot}6H_2O$ (0.0067 g, 0.015 mmol), $[Ru(tpyCOOH)_2](PF_6)_2$ (0.0048 g, 0.005 mmol), 1 mL DMF, 1 mL MeCN and 10 μL HCOOH. The mixture formed a homogenous solution at room temperature. The vial was placed and kept in a heating oven at 80 ℃ for 36 hours. After cooling to room

temperature, red needle crystals suitable for single crystal X-ray diffraction was obtained (2.0 mg), yield = 37.1% according to the mole amount of $[Ru(tpyCOOH)_2](PF_6)_2$. The needle crystals were washed with DMF for three times and soaked in MeCN for three days. The MeCN solvent was changed once per day. The red solid was collected and dried under vacuum at 80 ℃ overnight. Elemental analysis (%) of $\{1.5Eu\cdot 2[Ru(tpyCOO^-)_2]\cdot 2NO_3\cdot PF_6\cdot 1.5HCOO\cdot 16H_2O\}$, calcd. for $C_{65.5}H_{72.5}F_6N_{14}O_{33}PRu_2Eu_{1.5}$: C, 36.44; H, 3.39; N, 9.08; found: C, 36.70; H, 2.96; N, 8.67.

Synthesis of the Tb(III) coordination polymer (**Tb-Ru**). The procedure was same as that of **Eu-Ru** and $Tb(NO_3)_3\cdot 5H_2O$ was used as the metal precursor. **Tb-Ru** was afforded as red needle crystals, yield = 22.3% according to the mole amount of $[Ru(tpyCOOH)_2](PF_6)_2$. Elemental analysis (%) of $\{1.5Tb\cdot 2[Ru(tpyCOO^-)_2]\cdot 3NO_3\cdot 0.5PF_6\cdot HCOO\cdot DMF\cdot 13H_2O\}$, calcd. for $C_{68}H_{73}F_3N_{16}O_{33}P_{0.5}Ru_2Tb_{1.5}$: C, 37.89; H, 3.41; N, 10.04; found: C, 37.90; H, 3.08; N, 10.35.

Synthesis of the Yb(III) coordination polymer (**Yb-Ru**). The procedure was same as that of **Eu-Ru** and $Yb(NO_3)_3\cdot 6H_2O$ was used as the metal precursor. **Yb-Ru** was afforded as red needle crystals, yield = 34.2% according to the mole amount of $[Ru(tpyCOOH)_2](PF_6)_2$. Elemental analysis (%) of $\{1.5Yb\cdot 2[Ru(tpyCOO)_2]\cdot 3NO_3\cdot 0.5OH\cdot HCOO\cdot DMF\cdot 6H_2O\}$, calcd. for $C_{68}H_{59.5}N_{16}O_{26.5}Ru_2Yb_{1.5}$: C, 41.11; H, 3.02; N, 11.28; found: C, 41.56; H, 3.40; N, 10.88.

Synthesis of the Hf(IV) coordination polymer (**Hf-Ru**). A 5 mL glass solvothermal vial was charged with $HfCl_4$ (0.0128, 0.04mmol), $[Ru(tpyCOOH)_2](PF_6)_2$ (0.0096 g, 0.01 mmol), 2 mL DMF and 1 μL H_2O. The mixture formed a homogenous solution at room temperature. The vial was placed and kept in a heating oven at 135 ℃ for 24 hours. After cooling to room temperature, red plate crystals suitable for single crystal X-ray diffraction was obtained (2.1 mg), yield =22.8% according to the mole amount of $[Ru(tpyCOOH)_2](PF_6)_2$. The crystals were washed with DMF for three times and soaked in CH_2Cl_2 for three days. The CH_2Cl_2 solvent was changed once per day. The red solid was collected and dried under vacuum at 60 ℃ overnight. Elemental analysis (%) of $\{Hf\cdot[Ru(tpyCOO^-)_2]\cdot 2OH\cdot 2H_2O\cdot 2DMF\cdot PF_6\cdot Cl\}$, calcd. for $C_{39}H_{45}ClF_6N_8O_{10}PRuHf$: C, 37.60; H, 3.64; N, 8.99; found: C, 37.97; H, 2.83; N, 8.45.

Synthesis of the Zr(IV) coordination polymer **(Zr-Ru)**. The procedure was same as that of **Hf-Ru** and $ZrCl_4$ was used as the metal precursor. **Zr-Ru** was afforded as red plate crystals, yield =35.6% according to the mole amount of $[Ru(tpyCOOH)_2](PF_6)_2$. Elemental analysis (%) of $\{Zr\cdot[Ru(tpyCOO^-)_2]\cdot 2OH\cdot 2DMF\cdot PF_6\cdot Cl\}$, calcd. for $C_{38}H_{41}ClF_6N_8O_{10}PRuZr$: C, 39.95; H, 3.62; N, 10.9.81; found: C, 40.84; H, 3.13; N, 9.24.

X–ray Single Crystal Structure Determination

The cif files CCDC-2009804 (**Cu-Ru**), CCDC-2024242 (**Eu-Ru**), CCDC-2024244 (**Tb-Ru**), CCDC-2024245 (**Yb-Ru**), CCDC-2178964 **(Zr-Ru)** and CCDC-2178965 **(Hf-Ru)** contain the supplementary crystallographic data for this paper. The data can be obtained free of charge from Cambridge Crystallographic Data Centre, 12 Union Road, Cambridge, CB2 1EZ, UK (fax: ++44-1223-336-033; e-mail: deposit@ccdc.cam.ac.uk).

The dark red cuboid crystal (**Cu-Ru**), needle crystals (**Eu-Ru**, **Tb-Ru** and **Yb-Ru**) and plate crystals (**Zr-Ru** and **Hf-Ru**) suitable for crystal X-ray analysis were obtained by solvothermal methods (more details in the synthesis section above). Crystallographic data of **Eu-Ru** and **Tb-Ru** CPs were collected on SuperNova AtlasS2 diffractometer equipped with Mo *Kα* radiation (λ = 0.71073 Å) at 100.00(10) K. Data of **Cu-Ru**, **Zr-Ru**, **Hf-Ru** and **Yb-Ru** CPs were collected on SuperNova AtlasS2 diffractometer equipped with Cu *Kα* radiation (λ = 1.54178 Å) at 100.01(10) K. Absorption corrections were applied using the multi-scan program SADABS. All CP structures were solved using *SHELXT* structure solution program (Intrinsic Phasing) and refined by Least Squares procedures on F^2 using *SHELXL*.[2-3] Anisotropic thermal parameters were applied to all non-hydrogen atoms. Hydrogens on carbons of organic ligands were generated geometrically (C−H 0.95 Å); hydrogens of hydroxyl groups were located from different maps and refined with isotropic temperature factors. All hydrogen atoms in CP structures were placed in the position of optimized geometry. The DMF molecules in **Eu-Ru**, **Tb-Ru** and **Yb-Ru** can be identified via refinement of crystal data. However, it is hard to determine all anions around the positive units of CPs. Certain solvent molecules and anions that are particularly difficult to determine due to thermal vibration were removed by the *SQUEEZE* program of Platon.[4]

Single Crystal X-Ray Diffraction Data and Structural Parameters

Table S1. Crystallographic data, data collection and structure refinement details of **Cu-Ru**, **Eu-Ru**, **Tb-Ru**, **Yb-Ru**, **Zr-Ru**, and **Hf-Ru**.

Identification code	**Cu-Ru**	**Eu-Ru**	**Tb-Ru**	**Yb-Ru**	**Zr-Ru**	**Hf-Ru**
Empirical formula	$C_{70}H_{54}ClCu_2F_{17.14}N_{14}O_{10}P_3Ru_2$	$C_{65}H_{40}Eu_{1.5}N_{14}O_{16.24}Ru_2$	$C_{68}H_{47}N_{15}O_{17.1}Ru_2Tb_{1.5}$	$C_{68}H_{47}N_{15}O_{16.9}Ru_2Yb_{1.5}$	$C_{38}H_{38}N_8O_{10}RuZr$	$C_{38}H_{38}HfN_8O_{10}Ru$
Formula weight	2034.53	1707.07	1788.32	1806.34	959.05	1046.32
Temperature/K	214.00(12)	100.00(10)	100.01(10)	100.00(10)	99.98(10)	99.99(10)
Crystal system	monoclinic	monoclinic	monoclinic	monoclinic	triclinic	triclinic
Space group	*C*2/c	$P2_1/c$	$P2_1/c$	$P2_1/c$	*P*-1	*P*-1
a/Å	29.0186(3)	25.0292(8)	25.0025(7)	24.7189(11)	12.13920(10)	12.1240(2)
b/Å	18.7680(2)	8.5212(3)	8.5547(3)	8.5682(3)	13.41670(10)	13.4385(2)
c/Å	34.7051(3)	42.1166(15)	42.0897(12)	41.983(2)	14.45070(10)	14.4263(2)
α/°	90	90	90	90	110.6760(10)	110.702(2)
β/°	94.1800(10)	98.382(3)	98.273(3)	98.345(5)	90.0700(10)	90.1030(10)
γ/°	90	90	90	90	104.8810(10)	104.9950(10)
Volume/Å^3	18850.9(3)	8886.6(5)	8908.8(5)	8797.6(7)	2117.10(3)	2112.48(6)
Z	8	4	4	4	2	2
ρ_{calc}/g cm^{-3}	1.434	1.276	1.333	1.364	1.504	1.645
μ/mm^{-1}	4.590	1.438	1.573	6.110	5.448	7.893
F(000)	8114.0	3362.0	3529.0	3553.0	972.0	1036.0
Crystal size/mm^3	0.12×0.11×0.09	0.12 × 0.11 × 0.09	0.11 × 0.1 × 0.08	0.11 × 0.1 × 0.08	0.02 × 0.02 × 0.04	0.1 × 0.2 × 0.2
Radiation	Cu *Kα* (*λ* = 1.54184)	Mo *Kα* (*λ* = 0.71073)	Mo *Kα* (*λ* = 0.71073)	Cu *Kα* (*λ* = 1.54184)	Cu *Kα* (*λ* = 1.54184)	Cu *Kα* (*λ* = 1.54184)
2*θ* range for data collection/°	5.106 to 154.654	3.91 to 59.22	3.912 to 53.998	5.166 to 147.462	6.572 to 153.45	6.586 to 153.626
Index ranges	-36 ≤ h ≤ 36, -23 ≤ k ≤ 11, -42 ≤ l ≤ 43	-34 ≤ h ≤ 30, -11 ≤ k ≤ 7, -53 ≤ l ≤ 56	-31 ≤ h ≤ 28, -7 ≤ k ≤ 10, -53 ≤ l ≤ 41	-29 ≤ h ≤ 30, -10 ≤ k ≤ 10, -52 ≤ l ≤ 50	-15 ≤ h ≤ 14, -16 ≤ k ≤ l−6, -14 ≤ l ≤ 18	-15 ≤ h ≤ 15, -16 ≤ k ≤ 16, -18 ≤ l ≤ 17

Reflections collected	65143	47326	42061	62139	26983	25796
Independent reflections	19044 [R_{int} = 0.0345, R_{sigma} = 0.0329]	21263 [R_{int} = 0.0721, R_{sigma} = 0.1224]	19232 [R_{int} = 0.0570, R_{sigma} = 0.0997]	17439 [R_{int} = 0.1061, R_{sigma} = 0.0964]	8543 [R_{int} = 0.0411, R_{sigma} = 0.0415]	8500 [R_{int} = 0.0326, R_{sigma} = 0.0333]
Data/restraints/parameters	19044/0/1067	21263/0/893	19232/0/959	17439/0/970	8543/0/531	8500/0/531
Goodness-of-fit on F^2	1.041	1.008	1.016	1.022	1.084	1.119
Final R indexes [$I >= 2\sigma(I)$]	R_1 = 0.0803, wR_2 = 0.2424	R_1 = 0.0700, wR_2 = 0.1485	R_1 = 0.0624, wR_2 = 0.1258	R_1 = 0.0587, wR_2 = 0.1368	R_1 = 0.0646, wR_2 = 0.1978	R_1 = 0.0365, wR_2 = 0.0974
Final R indexes [all data]	R_1 = 0.0871, wR_2 = 0.2493	R_1 = 0.0998, wR_2 = 0.1646	R_1 = 0.0912, wR_2 = 0.1385	R_1 = 0.0799, wR_2 = 0.1497	R_1 = 0.0701, wR_2 = 0.2058	R_1 = 0.0394, wR_2 = 0.0992
Largest diff. peak/hole / e Å^{-3}	3.60/−1.70	3.29/−2.65	1.56/−1.85	1.37/−1.24	5.36/−0.84	2.04/−1.74

Table S2. Selected bond distances (Å) of **Cu-Ru**

Bond distance (Å)	**Cu-Ru**	Bond distance (Å)	**Cu-Ru**
Ru1-N2	1.978(4)	Cu2-Cu1	2.6389(11)
Ru1-N8[1]	1.981(5)	Cu2-O2	1.975(4)
Ru1-N9[1]	2.070(5)	Cu2-O7	1.970(4)
Ru1-N7[1]	2.075(5)	Cu2-O5	1.959(4)
Ru1-N3	2.085(6)	Cu2-O4	1.947(4)
Ru1-N1	2.069(6)	Cu2-O10	2.115(5)
Ru2-N11[2]	1.965(5)	Cu1-O1	1.960(4)
Ru2-N5	1.968(4)	Cu1-O6	1.986(4)
Ru2-N6	2.073(6)	Cu1-O3	1.965(3)
Ru2-N10[2]	2.081(6)	Cu1-O8	1.956(4)
Ru2-N12[2]	2.071(6)	Cu1-O9	2.114(5)
Ru2-N4	2.057(6)		
[1]+X,1-Y,-1/2+Z; [2]1/2+X,-1/2+Y,+Z			

Table S3. Selected bond distances (Å) of **Eu-Ru**, **Tb-Ru**, and **Yb-Ru** (M1 or M2 = Eu, Tb, or Yb).

Bond distance(Å)	**Eu- Ru**	**Tb- Ru**	**Yb- Ru**
Ru1-N2	1.972(5)	1.985(5)	1.983(5)
Ru1-N6	2.065(6)	2.065(6)	2.070(6)
Ru1-N1	2.076(5)	2.063(5)	2.071(6)
Ru1-N4	2.060(6)	2.059(6)	2.070(6)
Ru1-N5	1.980(5)	1.973(5)	1.983(5)
Ru1-N3	2.067(6)	2.071(5)	2.075(6)
Ru2-N8	1.976(5)	1.966(5)	1.980(5)
Ru2-N12	2.075(5)	2.056(5)	2.082(6)
Ru2-N7	2.060(5)	2.057(5)	2.067(6)
Ru2-N9	2.073(5)	2.071(5)	2.063(6)
Ru2-N10	2.059(6)	2.080(5)	2.064(6)
Ru2-N11	1.973(5)	1.972(5)	1.985(5)
M1-O11[1]	2.484(4)	2.456(4)	2.871(5)
M1-O11	2.741(4)	2.786(4)	2.349(5)
M1-O8	2.314(4)	2.288(4)	2.219(4)
M1-O9	2.488(6)	2.603(4)	2.373(5)
M1-O12	2.485(6)	2.451(4)	2.383(4)
M1-O10	2.598(5)	2.463(4)	2.593(6)
M2-O6[5]	2.247(5)	2.220(6)	2.241(9)
M2-O6	2.247(5)	2.220(6)	2.241(9)
M2-O4[5]	2.247(5)	2.280(9)	2.212(10)
M2-O4	2.247(5)	2.280(9)	2.212(10)
M2-O13[5]	2.528(14)	2.21(2)	2.374(19)
M2-O13	2.528(14)	2.21(2)	2.374(19)
M2-O14[5]	2.507(17)	2.449(13)	2.381(13)
M2-O14	2.507(17)	2.449(13)	2.381(13)
	[1]2-X,1/2+Y,1/2-Z; [2]1-X,1/2+Y,1/2-	[1]-X,-1/2+Y,3/2-Z; [2]-X,1/2+Y,3/2-	[1]-X,-1/2+Y,3/2-Z; [2]1-X,1/2+Y,3/2-Z; [3]-

Z; [3]1+X,1+Y,+Z; [4]2 -X,-1/2+Y,1/2- Z; [5]1-X,2-Y,1-Z	Z; [3]+X,1/2- Y,1/2+Z; [4]-X,-Y,1- Z; [5]1-X,1-Y,1-Z	1+X,1+Y,+Z; [4]1-X,1- Y,1-Z

Table S4. Selected bond distances (Å) of **Zr-Ru** and **Hf-Ru** (M1 = Zr or Hf).

Bond distance (Å)	**Zr-Ru**	**Hf-Ru**
Ru1-N5	1.984(4)	1.976(3)
Ru1-N6	2.061(5)	2.070(4)
Ru1-N1	1.973(4)	2.064(3)
Ru1-N4	2.066(5)	2.064(3)
Ru1-N3	2.078(4)	2.078(3)
Ru1-N2	2.064(4)	1.978(3)
M1-O8	2.012(3)	2.006(2)
M1-O5	1.990(3)	1.992(2)
M1-O7	1.979(3)	1.951(2)
M1-O6	1.953(3)	1.967(3)
M1-O2[1]	2.121(4)	2.105(3)
M1-O4	2.104(4)	2.092(3)
	[1]-1+X,-1+Y,+Z	[1]-1+X,-1+Y,+Z

Table S5. Selected bond angles (°) of **Cu-Ru**.

Bond angle (°)	**Cu-Ru**	Bond angle (°)	**Cu-Ru**
O1-Cu1-Cu2	83.07(12)	O2-Cu2-Cu1	82.43(12)
O1-Cu1-O6	88.49(17)	O2-Cu2-O10	98.85(19)
O1-Cu1-O3	89.00(16)	O7-Cu2-Cu1	82.25(13)
O1-Cu1-O9	97.76(19)	O7-Cu2-O2	164.63(18)
O6-Cu1-Cu2	83.75(12)	O7-Cu2-O10	96.48(19)
O6-Cu1-O9	93.88(19)	O5-Cu2-Cu1	82.35(12)
O3-Cu1-Cu2	81.30(12)	O5-Cu2-O2	89.36(16)
O3-Cu1-O6	165.04(17)	O5-Cu2-O7	89.89(17)
O3-Cu1-O9	101.08(18)	O5-Cu2-O10	97.17(18)
O8-Cu1-Cu2	84.37(13)	O4-Cu2-Cu1	84.58(13)
O8-Cu1-O1	167.35(18)	O4-Cu2-O2	88.38(17)
O8-Cu1-O6	88.57(17)	O4-Cu2-O7	88.89(18)
O8-Cu1-O3	90.68(17)	O4-Cu2-O5	166.92(18)
O8-Cu1-O9	94.7(2)	O4-Cu2-O10	95.91(19)
O9-Cu1-Cu2	177.47(15)	O10-Cu2-Cu1	178.64(15)

[1]+X,1-Y,-1/2+Z; [2]1/2+X,-1/2+Y,+Z; [3]+X,1-Y,1/2+Z; [4]-1/2+X,1/2+Y,+Z

Table S6. Selected bond angles (°) of lanthanide CPs (M1 or M2 = Eu, Tb, or Yb)

Bond angle (°)	**Eu-Ru**	**Tb-Ru**	**Yb-Ru**
O8-M1-O11	127.09(14)	126.63(13)	76.62(16)
O8-M1-O11[1]	75.25(14)	75.96(13)	126.31(14)
O8-M1-O9	122.6(2)	72.36(14)	122.60(17)
O8-M1-O12	81.07(18)	80.84(14)	80.61(16)
O8-M1-O10	72.58(15)	122.85(15)	72.27(17)
O6-M2-O14[5]	62.8(6)	90.9(4)	98.3(5)
O6[5]-M2-O14[5]	117.2(6)	89.1(4)	81.7(5)
O6-M2-O14	117.2(6)	89.1(4)	81.7(5)
O6[5]-M2-O14	62.8(6)	90.9(4)	98.3(5)
O6-M2-O13	63.9(5)	90.3(6)	80.6(5)
O6[5]-M2-O13[5]	63.9(5)	90.3(6)	80.6(5)
O6[5]-M2-O13	116.1(5)	89.7(6)	99.4(5)
O6-M2-O13[5]	116.1(5)	89.7(6)	99.4(5)
O4-M2-O14	91.0(4)	108.658(4)	107.8(9)
O4[5]-M2-O14[5]	91.0(4)	108.658(4)	107.8(9)
O4[5]-M2-O14	89.0(4)	71.342(4)	72.2(9)
O4-M2-O14[5]	89.0(4)	71.342(4)	72.2(9)
O4[5]-M2-O13	86.5(4)	123.7(5)	126.5(9)
O4[5]-M2-O13[5]	93.5(4)	56.3(5)	53.5(9)
O4-M2-O13[5]	86.5(4)	123.7(5)	126.5(9)
O4-M2-O13	93.5(4)	56.3(5)	53.5(9)
	[1]2-X,1/2+Y,1/2-Z; [2]1-X,1/2+Y,1/2-Z; [3]1+X,1+Y,+Z; [4]2-X,-1/2+Y,1/2-Z; [5]1-X,2-Y,1-Z; [6]1-X,-1/2+Y,1/2-Z; [7]-1+X,-1+Y,+Z	[1]-X,-1/2+Y,3/2-Z; [2]-X,1/2+Y,3/2-Z; [3]+X,1/2-Y,1/2+Z; [4]-X,-Y,1-Z; [5]1-X,1-Y,1-Z; [6]+X,1/2-Y,-1/2+Z	[1]-X,-1/2+Y,3/2-Z; [2]1-X,1/2+Y,3/2-Z; [3]-1+X,1+Y,+Z; [4]1-X,1-Y,1-Z; [5]-X,1/2+Y,3/2-Z; [6]1-X,-1/2+Y,3/2-Z; [7]1+X,-1+Y,+Z

Table S7. Selected bond angles (°) of **Zr-Ru** and **Hf-Ru** (M1 = Zr or Hf).

Bond angle (°)	**Zr-Ru**	**Hf-Ru**
O8-M1-O2[1]	90.31(15)	90.46(11)
O8-M1-O4	90.11(14)	90.72(11)
O5-M1-O8	177.17(14)	177.31(10)
O5-M1-O2[1]	90.73(14)	90.88(11)
O5-M1-O4	92.59(15)	91.70(11)
O7-M1-O8	87.68(14)	86.72(11)
O7-M1-O5	89.74(14)	92.09(11)
O7-M1-O2[1]	87.06(16)	175.33(11)
O7-M1-O4	172.63(16)	90.34(12)
O6-M1-O8	87.10(15)	87.55(11)
O6-M1-O5	92.04(14)	90.19(11)
O6-M1-O7	96.69(16)	96.35(12)
O6-M1-O2[1]	175.34(16)	87.24(12)
O6-M1-O4	90.21(16)	172.98(12)
O4-M1-O2[1]	85.93(16)	85.97(12)
	[1]-1+X,-1+Y,+Z; [2]1+X,1+Y,+Z	[1]-1+X,-1+Y,+Z; [2]1+X,1+Y,+Z

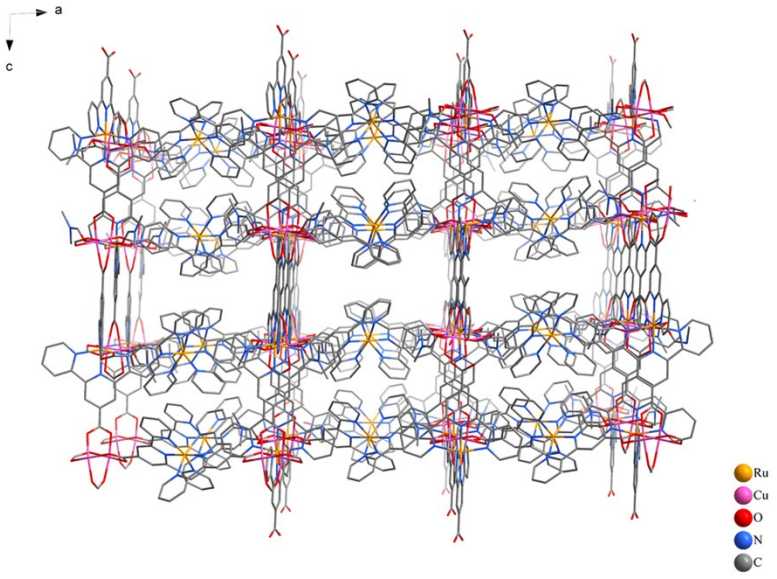

Figure S1. The 3D network of **Cu-Ru** viewed along the *b* axis.

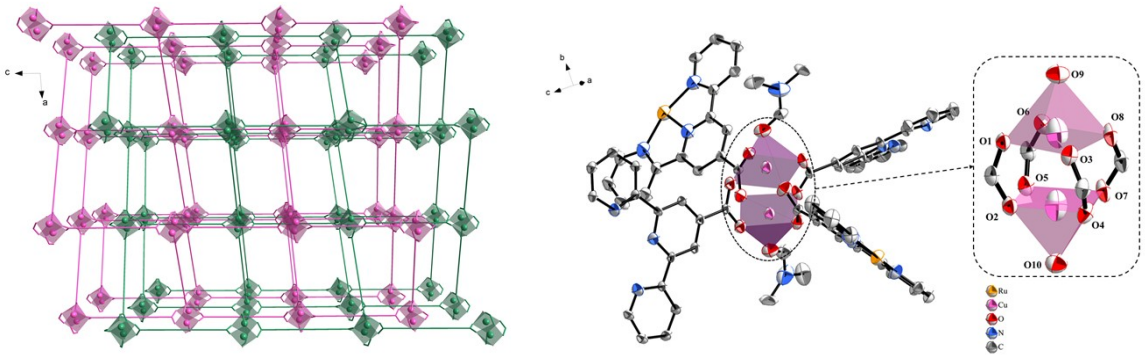

Figure S2. Left. Representation of the interpenetrated structure of **Cu-Ru**, where the polyhedron represents coper nodes. Right. The coordination environment of copper cations in **Cu-Ru**, with atom numbers.

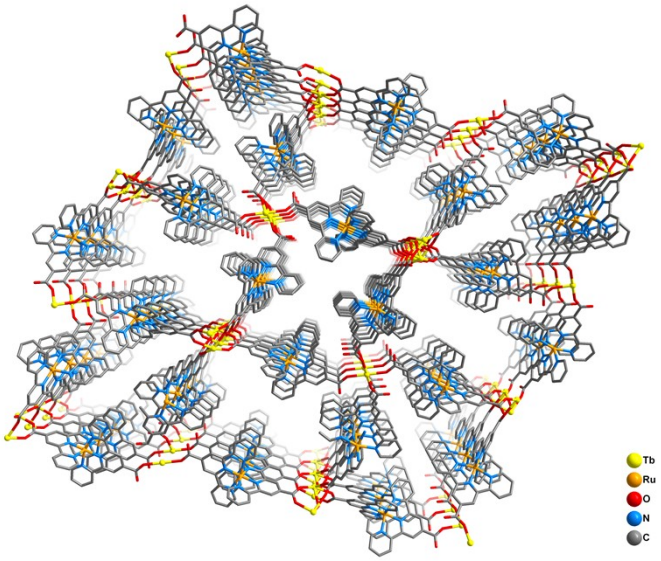

Figure S3. 3D network of **Tb-Ru** viewed along the *b* axis.

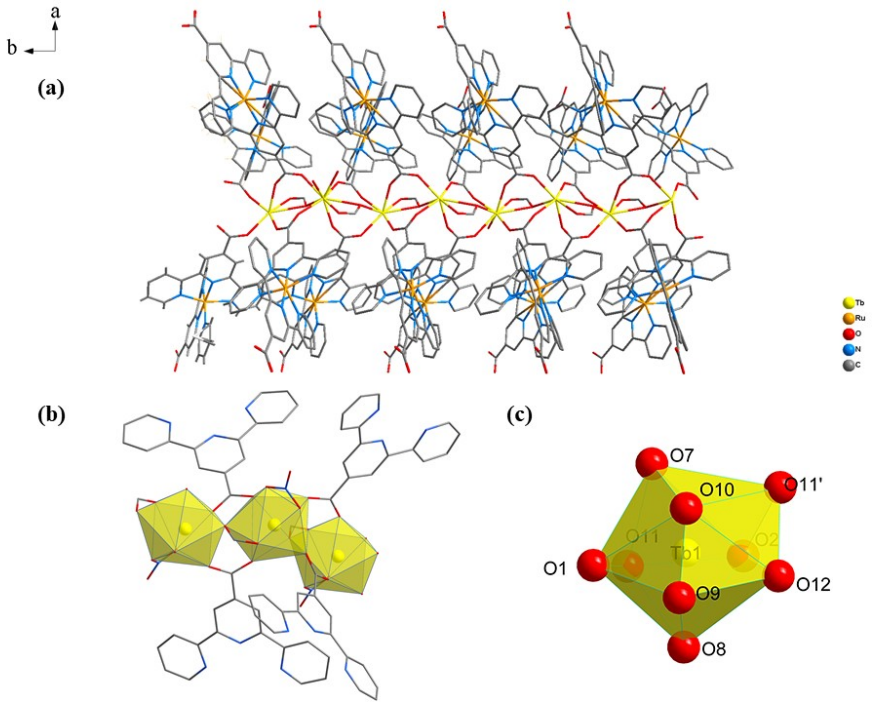

Figure S4. (a) The coordination chain of terbium nodes (drawn as yellow polyhedrons) in **Tb-Ru**. (b) Coordination modes of the Tb1 nodes and [Ru(tpyCOO^{-})$_2$] linkers. (c) The Tb1 ion polyhedron with atom numbers.

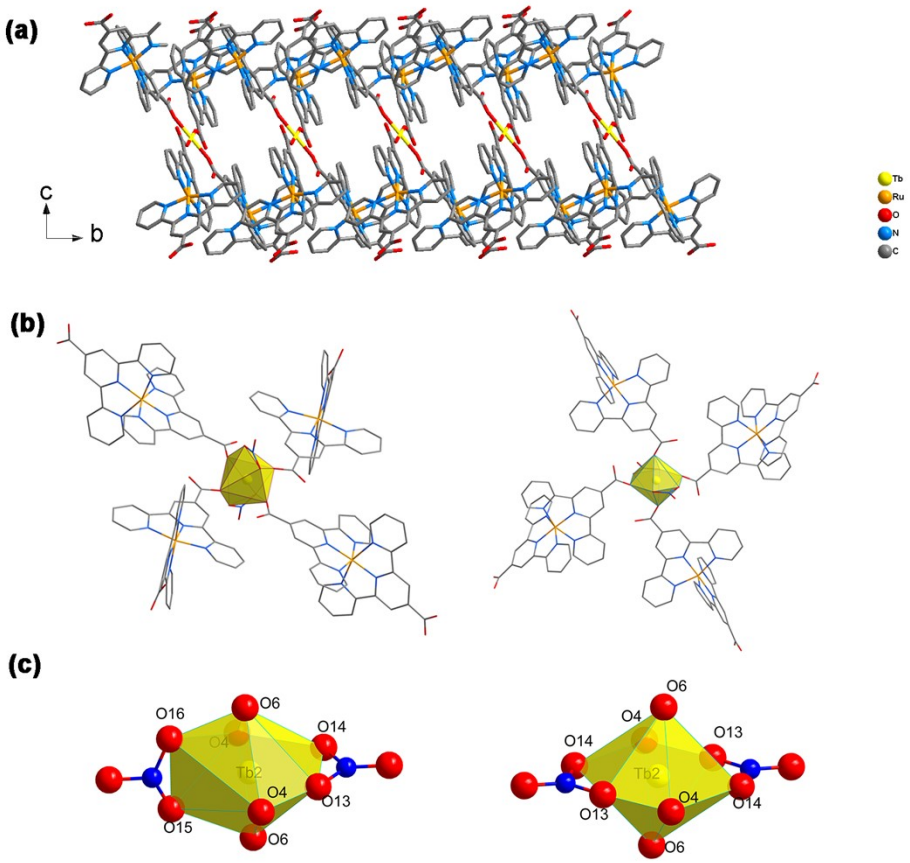

Figure S5. (a) The coordination chain of terbium nodes (drawn as yellow polyhedrons) in **Tb-Ru**. The coordinated nitrates are omitted. (b) Coordination modes of the Tb2 nodes and [Ru(tpyCOO^{-})$_2$] linkers. (c) Tb2 ion polyhedrons with atom numbers.

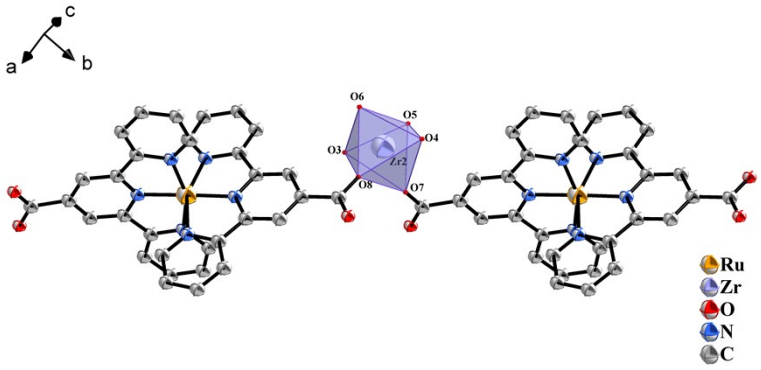

Figure S6. The coordination environment of zirconium cations in **Zr-Ru** with atom numbers.

Powder X-Ray Diffraction Data

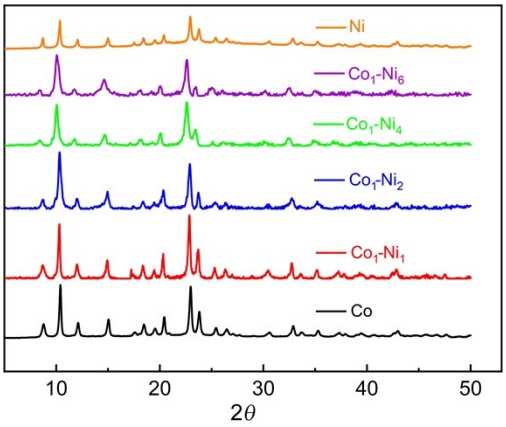

Figure S7. PXRD patterns of bimetallic **Co_x-Ni_y-Ru** coordination polymers, and **Ni-Ru** and **Co-Ru** coordination polymers.[1] The samples were dried under vacuum (see syntheses section) before measurement.

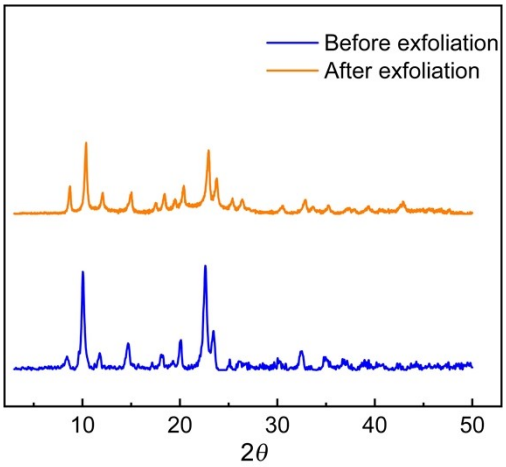

Figure S8. PXRD patterns of bimetallic **Co_1-Ni_4-MOF** before and after exfoliation.

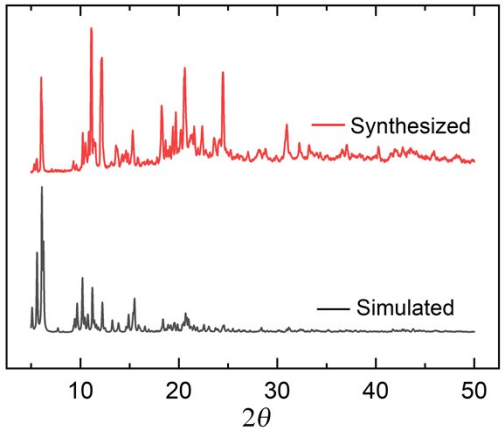

Figure S9. PXRD patterns of **Cu-Ru**. The samples were dried under vacuum (see syntheses section) before measurement. The simulated profile derives from the single-crystal data of **Cu-Ru**.

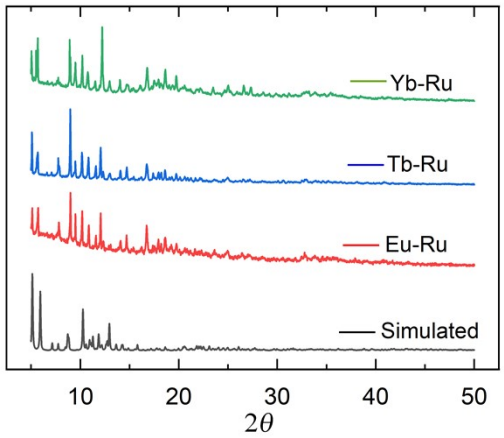

Figure S10. PXRD patterns of **Tb-Ru**, **Yb-Ru** and **Eu-Ru** coordination polymers. The samples were dried under vacuum (see syntheses section) before measurement. The simulated profile derives from the single-crystal data of **Tb-Ru**.

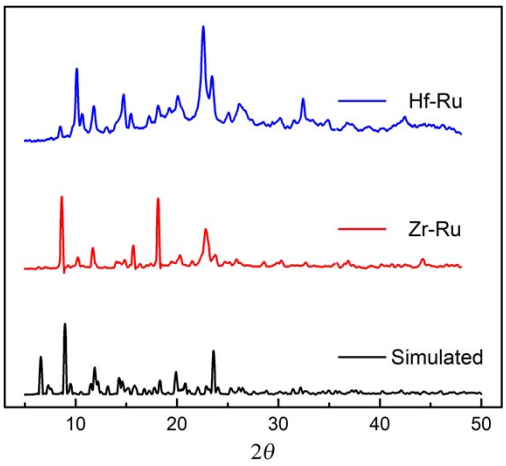

Figure S11. PXRD patterns of **Zr-Ru** and **Hf-Ru** coordination polymers.

SEM Images

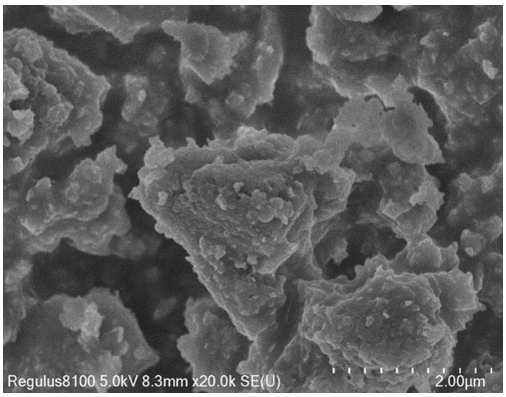

Figure S12. FE-SEM images of **Co_1-Ni_2-Ru** before exfoliation.

TEM images

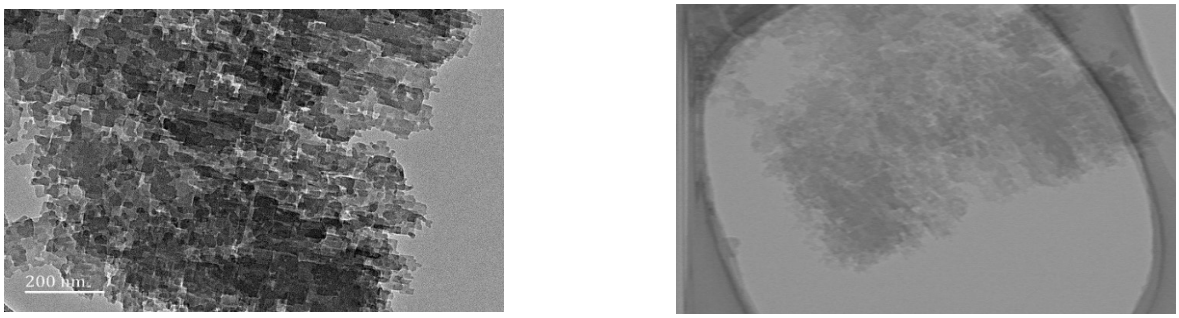

Figure S13. TEM images of **Co_1-Ni_2-Ru** nanosheets (left and right).

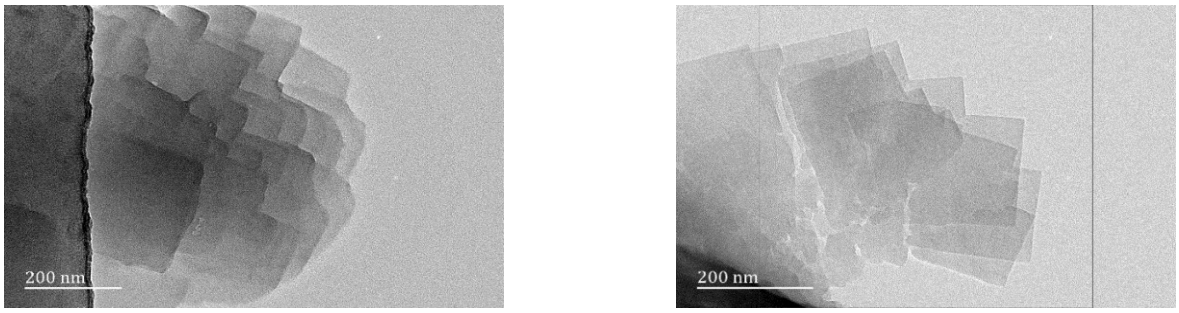

Figure S14. TEM images of **Co_1-Ni_6-Ru** nanosheets (left and right).

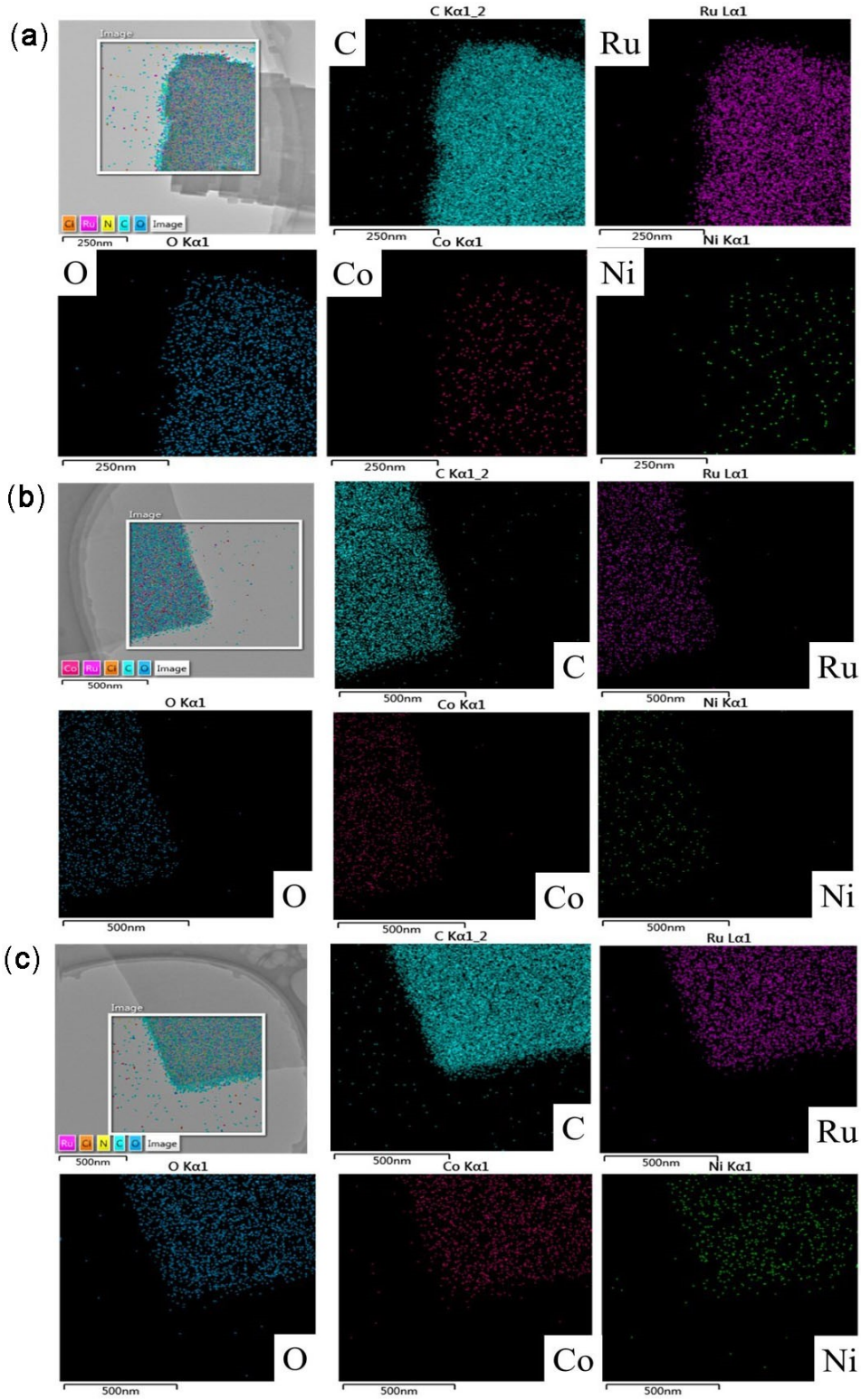

Figure S15. TEM images and elemental mapping of exfoliated **Co_1-Ni_1-Ru** (a), **Co_1-Ni_4-Ru** (b), and **Co_1-Ni_6-Ru** (c) nanosheets.

ICP-MS

Table S8. Co and Ni element compositions of different bimetallic CPs

Sample	Content of Co (wt.%)	Content of Ni (wt.%)	n(Co)/n(Ni)
Co_1-Ni_1-Ru	6.26	0.41	15.21
Co_1-Ni_2-Ru	4.85	1.03	4.69
Co_1-Ni_4-Ru	4.18	1.95	2.14
Co_1-Ni_6-Ru	3.97	2.29	1.73

X-ray Photoelectron Spectroscopy (XPS)

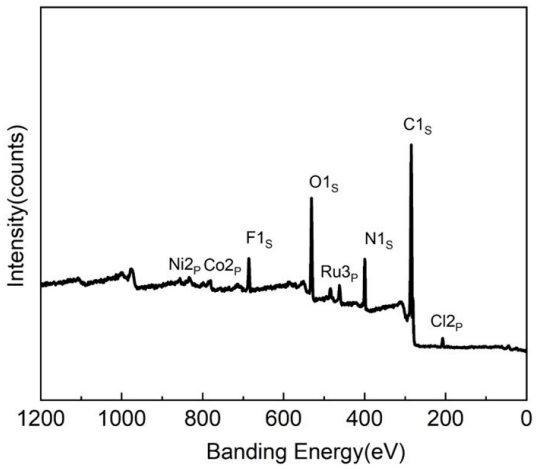

Figure S16. The XPS spectrum of **Co_1-Ni_4-Ru**.

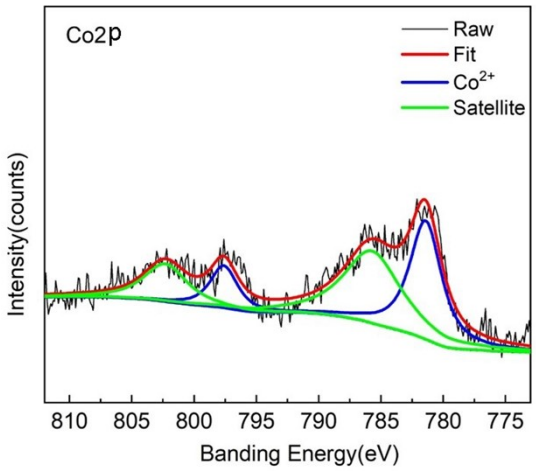

Figure S17. The XPS Co 2p scan for **Co_1-Ni_4-Ru**.

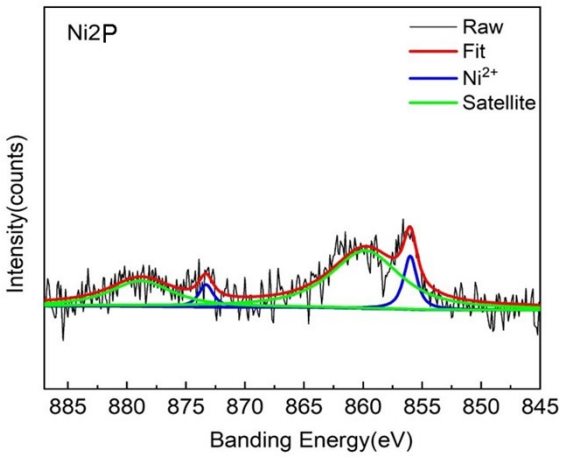

Figure S18. The XPS Ni 2p scan for **Co_1-Ni_4-Ru**.

Thermogravimetric Analysis (TGA)

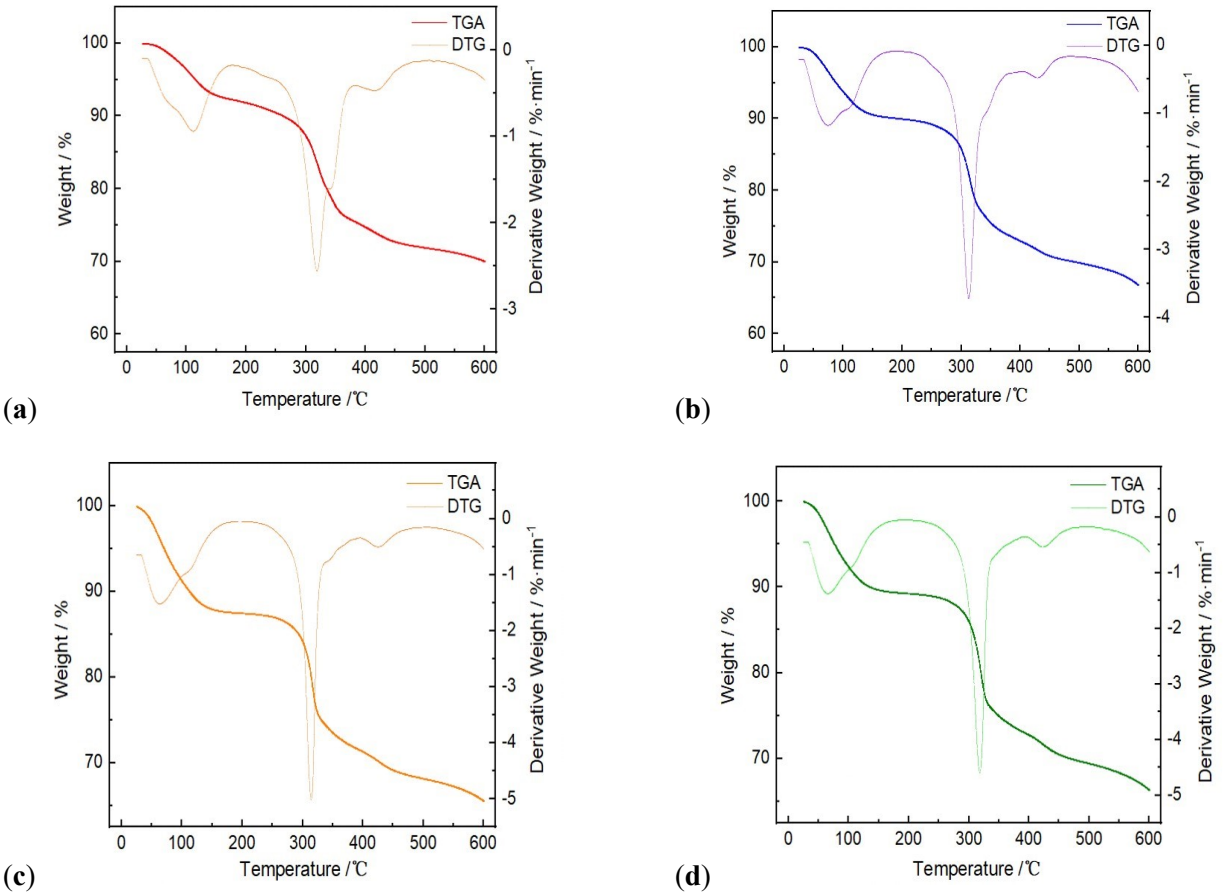

Figure S19. TGA and DTG curves of **Co_1-Ni_1-Ru** (a), **Co_1-Ni_2-Ru** (b), **Co_1-Ni_4-Ru** (c), **Co_1-Ni_6-Ru** (d) coordination polymers.

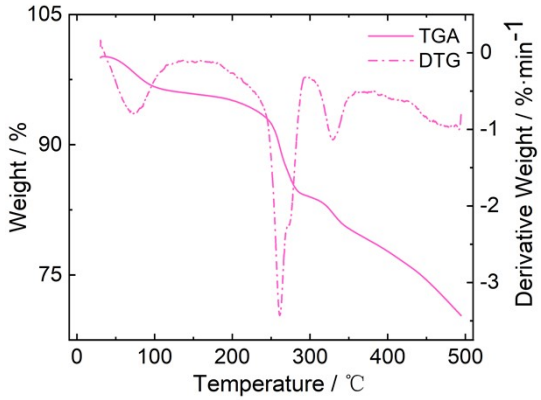

Figure S20. TGA and DTG curves of **Cu-Ru** coordination polymer.

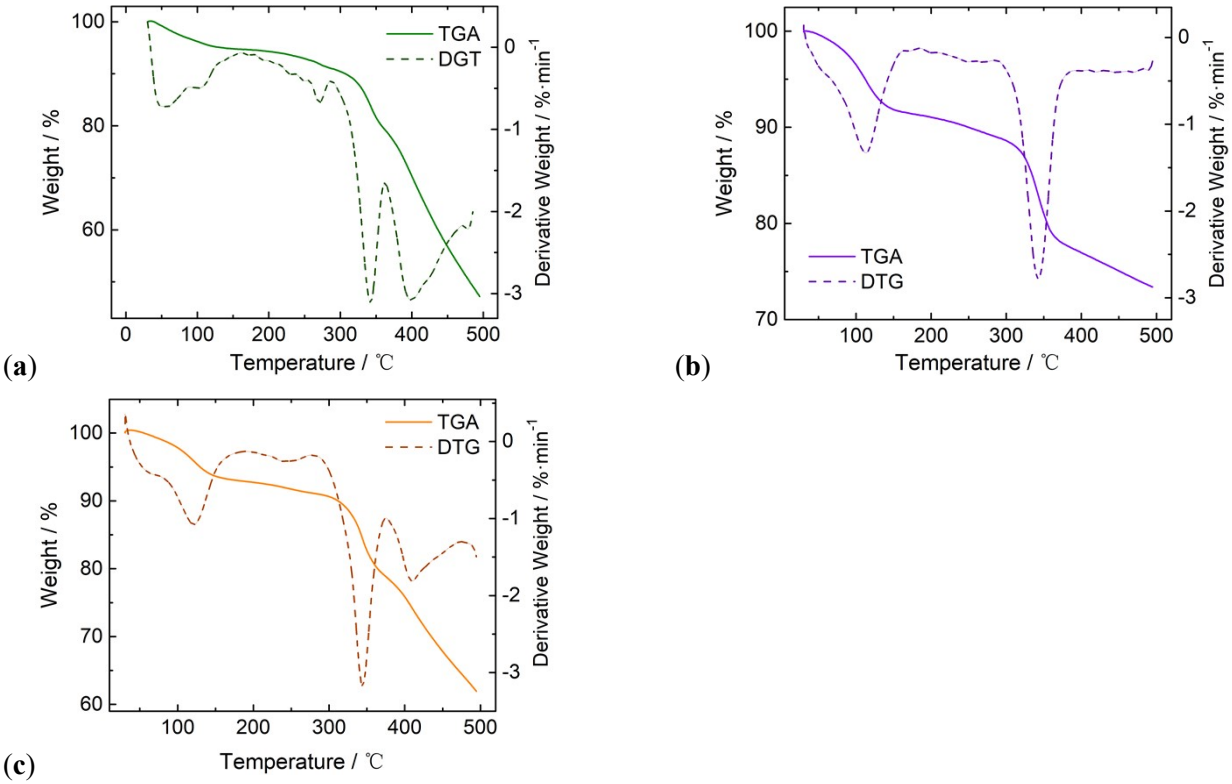

Figure S21. TGA and DTG curves of **Eu-Ru** (a), **Tb-Ru** (b), **Yb-Ru** (c) coordination polymers.

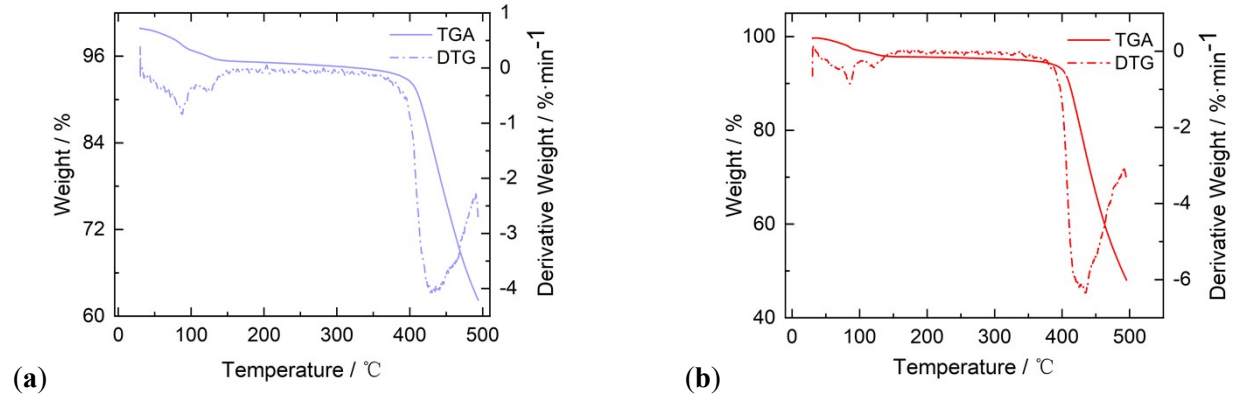

Figure S22. TGA and DTG curves of **Zr-Ru** (a) and **Hf-Ru** (b) coordination polymers.

N_2 Gas sorption isotherms

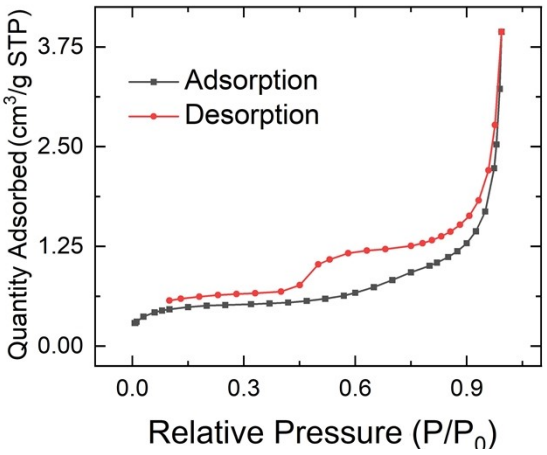

Figure S23. N_2 adsorption and desorption isotherms of **Cu-Ru** at 77 K.

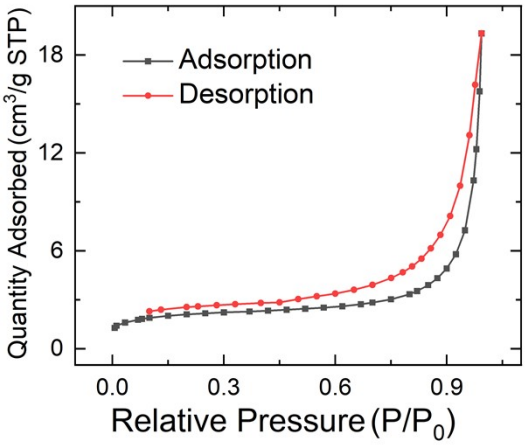

Figure S24. N_2 adsorption and desorption isotherms of **Yb-Ru** at 77 K.

Electrochemical Properties

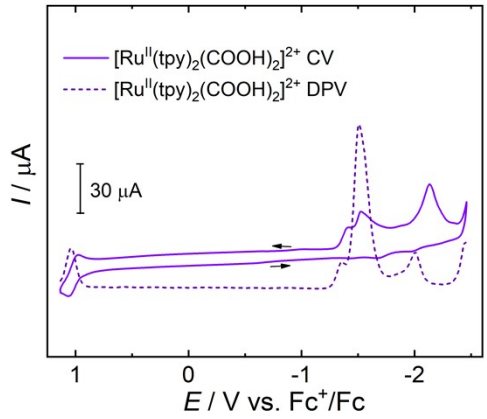

Figure S25. CV and DPV of $[Ru(tpyCOOH)_2](PF_6)_2$ in an acetonitrile solution of Bu_4NPF_6 (0.1 M) at a scan rate of 100 mV/s.[1]

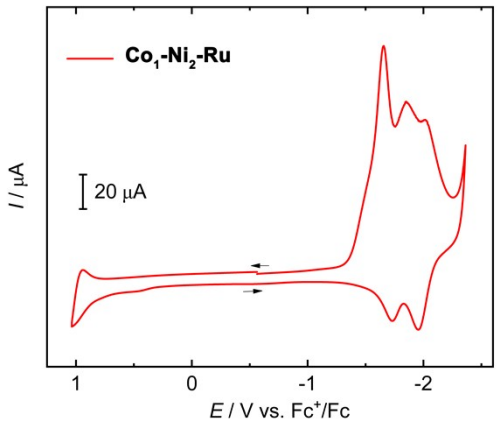

Figure S26. CV of **Co_1-Ni_2-Ru** in an acetonitrile solution of Bu_4NPF_6 (0.1 M) at a scan rate of 100 mV/s.

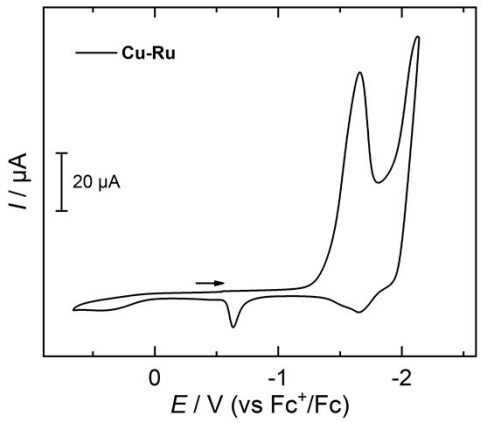

Figure S27. CV of **Cu-Ru** in an acetonitrile solution of Bu_4NPF_6 (0.1 M) at a scan rate of 100 mV/s.

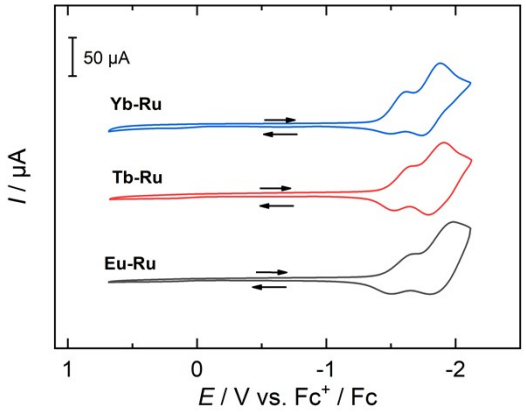

Figure S28. CVs of **Eu-Ru**, **Tb-Ru**, and **Yb-Ru** in an acetonitrile solution of Bu_4NPF_6 (0.1 M) at a scan rate of 100 mV/s.

Photochemical Properties

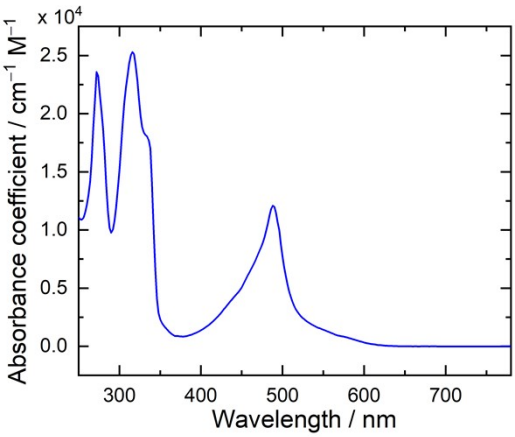

Figure S29. UV−vis absorbance spectrum of 0.05 mM $[Ru(tpyCOOH)_2](PF_6)_2$ in acetonitrile.

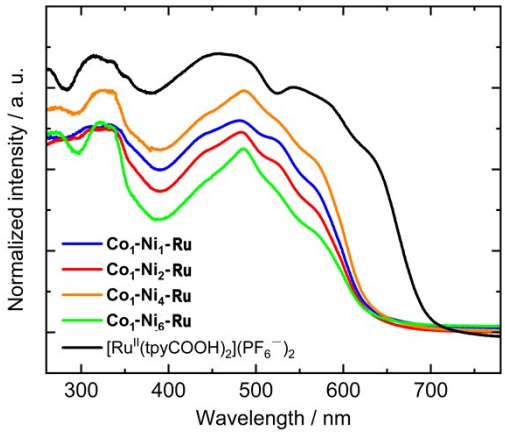

Figure S30. Normalized UV−vis absorbance spectra bimetallic Co/Ni CPs and $[Ru(tpyCOOH)_2](PF_6)_2$ in their solid state.

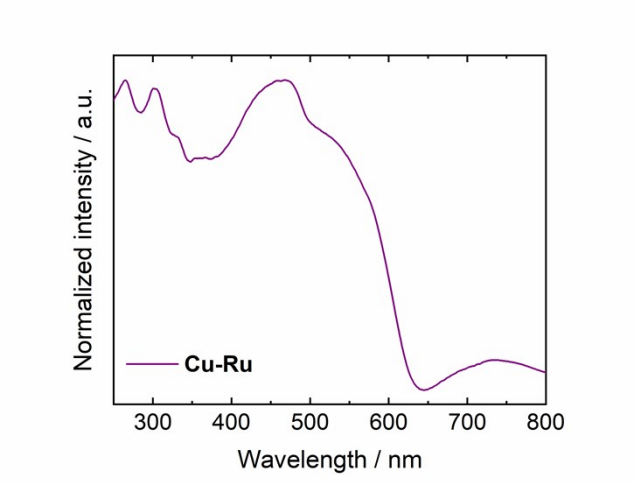

Figure S31. Normalized UV−vis absorbance spectrum of **Cu-Ru** in its solid state.

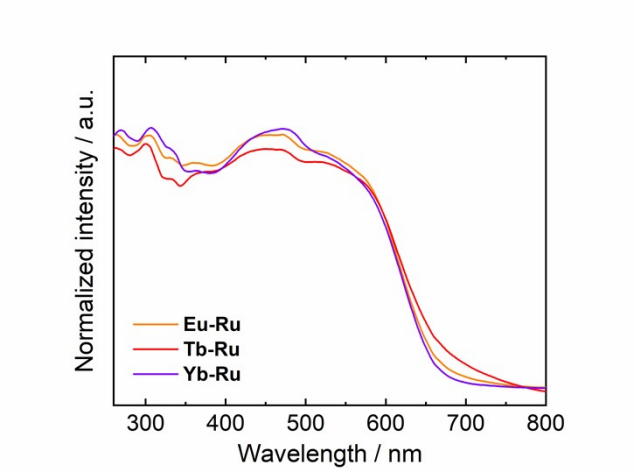

Figure S32. Normalized UV−vis absorbance spectra of **Eu-Ru**, **Tb-Ru**, and **Yb-Ru** in their solid state.

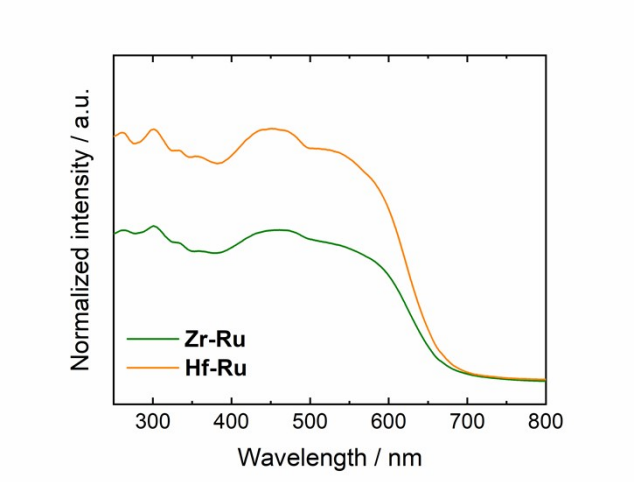

Figure S33. Normalized UV−vis absorbance spectra of **Zr-Ru** and **Hf-Ru** in their solid state.

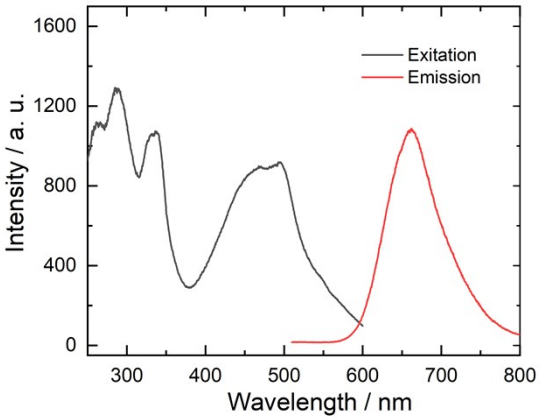

Figure S34. The excitation (gray, λ_{em} = 650 nm) and emission (red, λ_{ex} = 480 nm) spectra of 0.05 mM $[Ru(tpyCOOH)_2](PF_6)_2$ in acetonitrile.

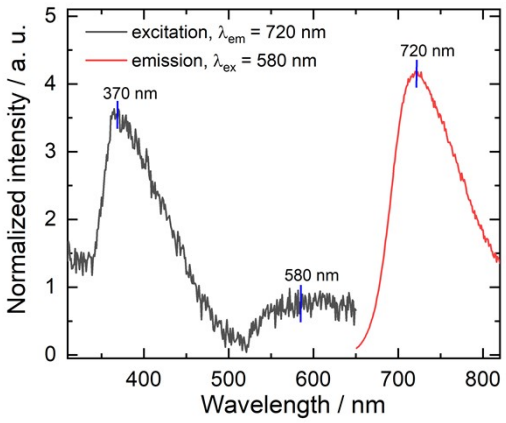

Figure S35. Excitation (gray, λ_{em} = 720 nm) and emission (red, λ_{ex} = 580 nm) spectra of $[Ru(tpyCOOH)_2](PF_6)_2$ solid powder.

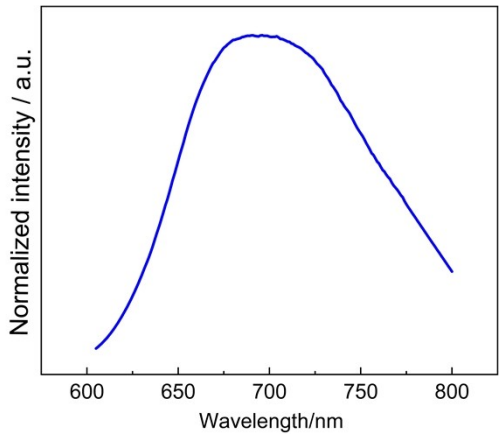

Figure S36. The emission spectrum of **Co_1-Ni_2-Ru** in solid state, excited at λ_{ex} = 580 nm.

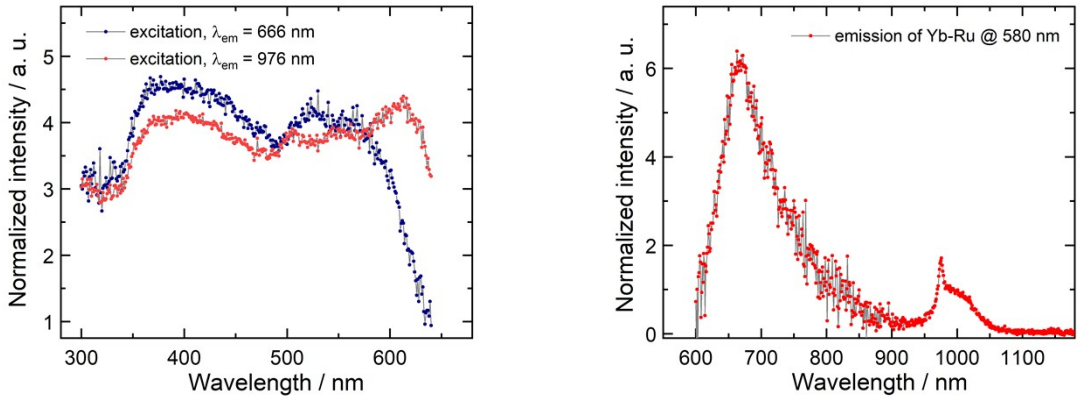

Figure S37. Excitation (left) and emission (right) spectra of MOF **Yb-Ru** solid powder.

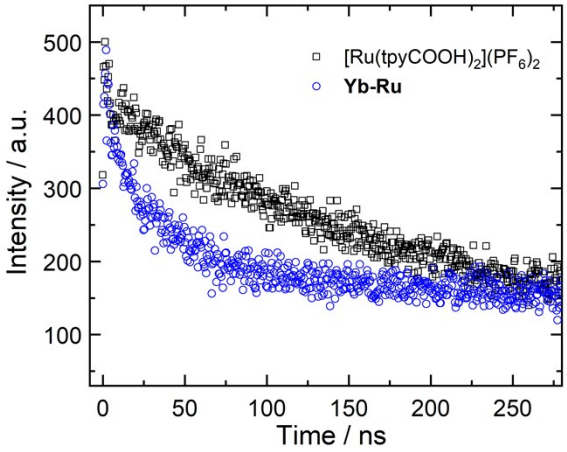

Figure S38. The photoluminescent decay traces of solid **Yb-Ru** (blue circles, λ_{em} = 666 nm) and $[Ru(tpyCOOH)_2](PF_6)_2$ (black squares, λ_{em} = 719 nm) during the initial 275 ns period (λ_{ex} = 365 nm).

Photocatalytic Hydrogen Evolution

In a typical trial of photocatalytic hydrogen evolution experiment, the catalyst sample was prepared by adding 60 mg CP solid and 30 mL deionized water into a 100 mL thick wall beaker. The bulky CP crystalline solid was dispersed by ultrasonicating at 0 ℃ for an hour, affording a suspension of CP particles (2 mg mL^{-1}). The suspension was mixed with another 30 mL ascorbic acid solution (1.0 mol L^{-1}), and the pH of the mixture was adjusted to certain value by addition of sodium hydroxide. The mixture was then transferred to a 270 mL photocatalytic glass reactor and bubbled with argon gas under stirring for 30 min. Photocatalytic hydrogen evolution was conducted by irradiating the suspension with a 300W Xenon lamp (Perfect Light PLS-SXE 300) through a 420 nm cut-off filter. The amount of hydrogen generation was quantified by a gas chromatography (GC, SHIMADZU GC-2018) with a 5Å molecular sieve column (2 × 3 mm, 60–80 mesh), Ar carrier gas and a TCD detector. The reported values of hydrogen amount were average of three independent trials. The initial photocatalytic rates were calculated according to the hydrogen evolution during the incipient 30 min.

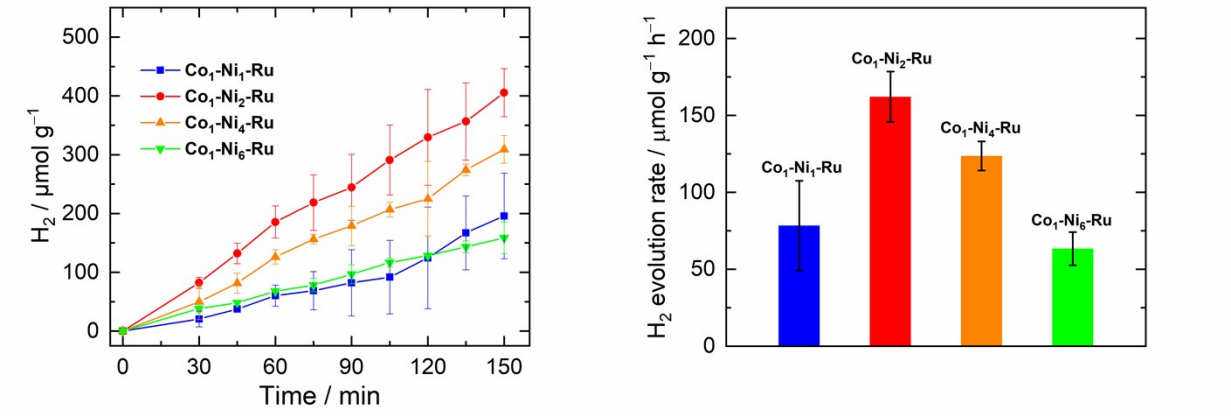

Figure S39. Left: Photocatalytic hydrogen evolution by 2D bimetallic Co/Ni CPs under visible-light irradiation (> 420 nm) from ascorbic acid solution (0.5 M, pH = 3.0). Right: Initial photocatalytic hydrogen evolution rates (μmol g^{-1} h^{-1}) for different 2D bimetallic Co/Ni nanosheets.

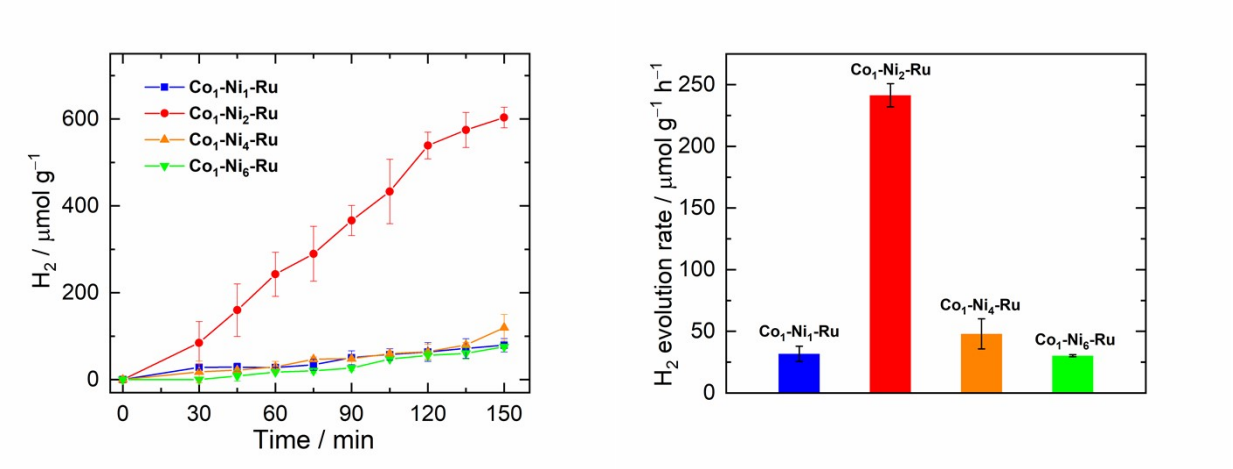

Figure S40. Left: Photocatalytic hydrogen evolution by 2D bimetallic Co/Ni CPs under visible-light irradiation (> 420 nm) from ascorbic acid solution (0.5 M, pH = 5.0). Right: Initial photocatalytic hydrogen evolution rates (μmol g^{-1} h^{-1}) for different 2D bimetallic Co/Ni CPs.

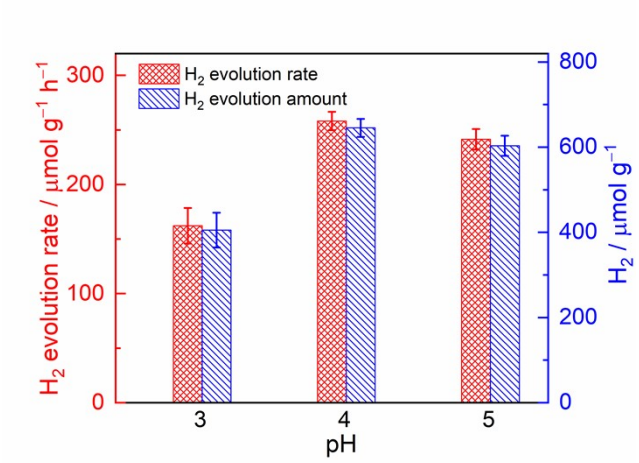

Figure S41. Photocatalytic hydrogen evolution rates and amounts (after 150 min) by **Co_1-Ni_2-Ru** CP under visible-light irradiation (> 420 nm) from ascorbic acid solution at different pH values.

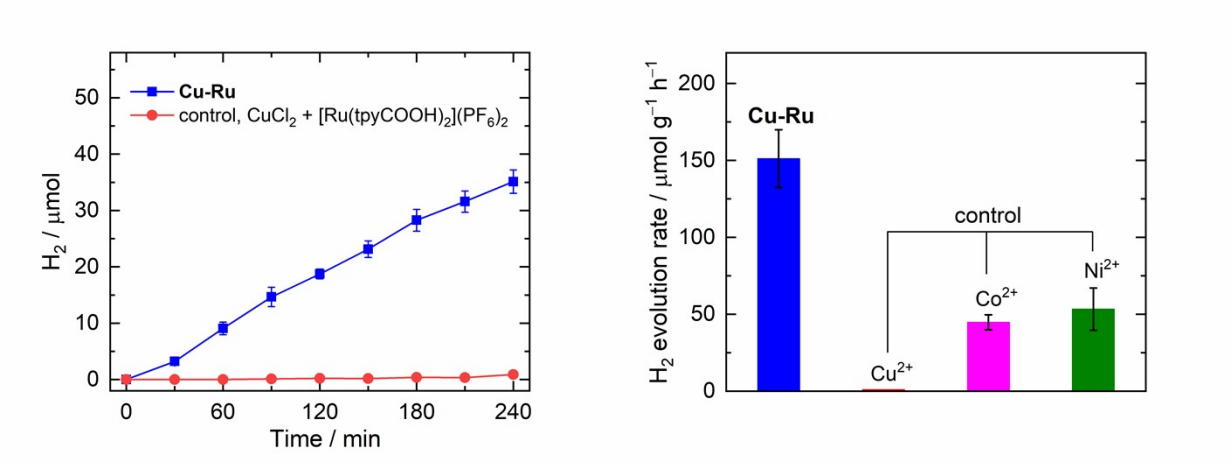

Figure S42. Left: Photocatalytic hydrogen evolution by **Cu-Ru** under visible-light irradiation (> 420 nm) from ascorbic acid solution (0.5 M, pH = 4.0). Right: Initial photocatalytic hydrogen evolution rates (μmol g^{-1} h^{-1}) for **Cu-Ru** and the control experiment, where stoichiometric $CuCl_2 \cdot 6H_2O$ and $[Ru(tpyCOOH)_2](PF_6)_2$ were applied as the alternative of **Cu-Ru**. The data of Co^{2+} and Ni^{2+} control experiments were referred to the previous report.[1]

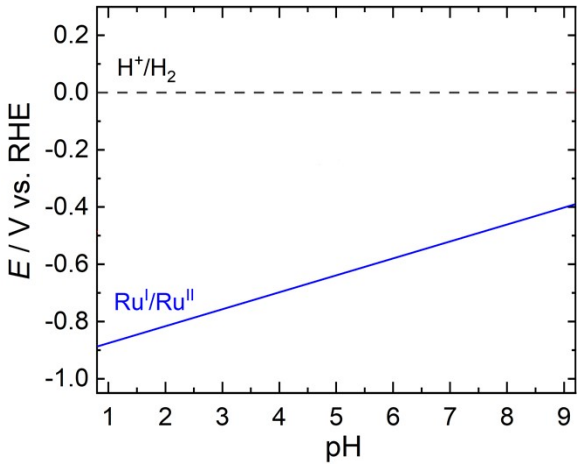

Figure S43. Estimated redox potentials (V vs. RHE) of the [Ru ($tpyCOO^-$)$_2$] linker in 2D CPs at the formal Ru(I) state. The redox potentials were referred to the previous report.[1]

References

1. Huo, D.; Lin, F.; Chen, S.; Ni, Y.; Wang, R.; Chen, H.; Duan, L.; Ji, Y.; Zhou, A.; Tong, L., Ruthenium Complex-Incorporated Two-Dimensional Metal-Organic Frameworks for Cocatalyst-Free Photocatalytic Proton Reduction from Water. *Inorg. Chem.* **2020,** *59* (4), 2379-2386.
2. Dolomanov, O. V.; Bourhis, L. J.; Gildea, R. J.; Howard, J. A. K.; Puschmann, H., OLEX2: a complete structure solution, refinement and analysis program. *J. Appl. Cryst.* **2009,** *42* (2), 339-341.
3. Sheldrick, G., A short history of SHELX. *Acta Crystallogr. Sect. A* **2008,** *64* (1), 112-122.
4. Spek, A., PLATON SQUEEZE: a tool for the calculation of the disordered solvent contribution to the calculated structure factors. *Acta Crystallogr. Sec. C* **2015,** *71* (1), 9-18.